ACS APPLIED MATERIALS & INTERFACES

Research Article

www.acsami.org

Role of Capsular Polysaccharides in Biofilm Formation: An AFM Nanomechanics Study

Huabin Wang,[†,§] Jonathan J. Wilksch,[‡] Richard A. Strugnell,*[,‡] and Michelle L. Gee[†]

[†]Department of Chemistry and [‡]Department of Microbiology and Immunology, University of Melbourne, Parkville, Victoria 3010, Australia

[§]Chongqing Key Laboratory of Multi-Scale Manufacturing Technology, Chongqing Institute of Green and Intelligent Technology, Chinese Academy of Sciences, Chongqing 400714, China

Supporting Information

ABSTRACT: Bacteria form biofilms to facilitate colonization of biotic and abiotic surfaces, and biofilm formation on indwelling medical devices is a common cause of hospital-acquired infection. Although it is well-recognized that the exopolysaccharide capsule is one of the key bacterial components for biofilm formation, the underlying biophysical mechanism is poorly understood. In the present study, nanomechanical measurements of wild type and specific mutants of the pathogen, *Klebsiella pneumoniae*, were performed *in situ* using atomic force microscopy (AFM). Theoretical modeling of the mechanical data and static microtiter plate biofilm assays show that the organization of the capsule can influence bacterial adhesion, and thereby biofilm formation. The capsular organization is affected by the presence of type 3 fimbriae. Understanding the biophysical mechanisms for the impact of the structural organization of the bacterial polysaccharide capsule on biofilm formation will aid the development of strategies to prevent biofilm formation.

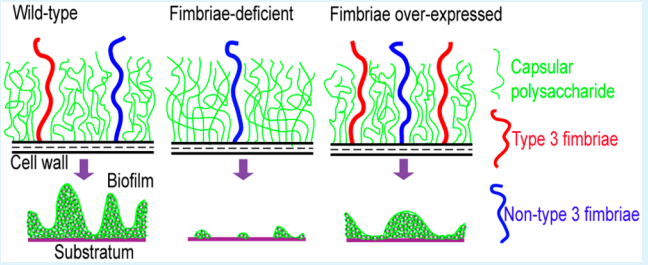

KEYWORDS: *bacteria, capsule, polysaccharides, fimbriae, biofilm, nanomechanics*

INTRODUCTION

The evolution of antibiotic-resistant bacteria, or "superbugs" as they are often called, is one of the biggest global health issues of the 21st century. Drug resistance is now a feature of many bacterial pathogens. Many of these bacteria are opportunistic: they can cause a wide range of nosocomial (hospital-acquired) infections associated with the formation of bacterial biofilm on both biotic and abiotic surfaces such as wounds, medical equipment such as catheters, and artificial implants such as pacemakers and artificial joints.[1−3] Bacterial adhesion to a substrate is the first essential step for biofilm formation. Fimbriae, also called pili, are proteinaceous structures that radiate from the bacterial cell surface to a distance of approximately 100 nm to several microns and consist of adhesins that are thought to facilitate bacterial adhesion.[4−6] There are many different types of fimbriae, which can be differentiated by the protein constituents and the genes encoding these proteins.[1] Surface polysaccharides also encapsulate many bacterial species such as *Acinetobacter baumannii* and *Klebsiella pneumoniae*, which are both opportunistic bacteria commonly associated with hospital-acquired infections. Little is known, however, regarding the interplay between fimbriae and capsule in the formation of biofilms.

Traditionally, cell surface components implicated in biofilm formation have been studied using a variety of techniques drawn from microbiology, immunology, and molecular biology.[7,8] However, it is difficult to use these approaches to elucidate the fundamental biophysical mechanisms of various components contributing to biofilm formation.[7,9] Atomic force microscopy (AFM) is a powerful tool in single-cell microbiology, enabling live bacterial cell imaging in physiologically relevant environments, and probing the physical properties of cell interactions.[10,11] AFM has been widely used to measure the cell wall elasticity, to identify molecular recognition sites, to explore the mechanical properties of cell surface polymers, and to investigate cell adhesion.[12−16] Although these studies have greatly enhanced our understanding of cell−surface interactions, the biophysical mechanisms underlying the function of bacterial surface components in biofilm formation remain largely unknown. This is due to the biochemical and biophysical complexity of cell surface structures and the difficulty in interpreting nanoscale interactions between an AFM tip and a bacterial surface.[2,17]

In our recent work, we established an AFM nanomechanics method for probing cell viability and the organization and structure of the bacterial cell wall and surface polymers. We revealed a biophysical mechanism by which the polysaccharide capsule protects the bacterial cell from environmental stresses.[18] In the present study, we have used this method to

Received: April 8, 2015
Accepted: May 26, 2015
Published: June 2, 2015

DOI: 10.1021/acsami.5b03041
ACS Appl. Mater. Interfaces 2015, 7, 13007−13013

explore the interactions between fimbriae and capsule polysaccharides in the formation of a *K. pneumoniae* biofilm. We correlated bacterial surface structures with the ability to form biofilms, for encapsulated wild type *K. pneumoniae* strain AJ218 and a series of specific AJ218 mutants: bacteria deficient in type 3 fimbriae, bacteria where type 3 fimbriae were overexpressed, and bacteria deficient in capsule production. Our results show that biofilm formation is assisted by the fluidity of the capsular polysaccharides and that fimbriae help maintain this fluidity.

EXPERIMENTAL SECTION

Bacterial Strains, Culture Conditions, and Harvesting. *K. pneumoniae* AJ218 (capsule serotype K54) is a human urinary tract infection isolate.[19] All strains were cultured on Luria–Bertani (LB) agar at 37 °C. These cultures were used to inoculate LB broths which were grown for 16 h at 37 °C while shaking (180 rpm). Stationary-phase cells were subsequently harvested by centrifugation (10 min at 3500 × *g*) and washed twice with Milli-Q water (18.2 MΩ cm^{-1}). The final concentration of cells in Milli-Q water was approximately 2×10^8 CFU/mL. Kanamycin (50 μg/mL) was used to select for growth of type 3 fimbriae-deficient and capsule-deficient mutants, while chloramphenicol (60 μg/mL) was used to select for type 3 fimbriae overexpressed strains.

A type 3 fimbriae knockout mutant, in which the *mrkA* gene encoding the major fimbrial subunit was deleted and replaced with a kanamycin resistance cassette (*km*), was constructed in *K. pneumoniae* AJ218, as described previously.[8] *K. pneumoniae* AJ218 which overexpressed type 3 fimbriae contained a plasmid vector carrying the *mrkABCDF* operon (pMrk), as described previously.[8] A *wzc* mutant deficient in capsule polysaccharide export was isolated following random mini-Tn*5Km2* transposon insertion mutagenesis of *K. pneumoniae* AJ218.[8,20]

Static Biofilm Assays. Biofilm assays were performed as described previously.[8] Briefly, bacterial cultures were grown in M63B1-GCAA minimal media (containing 1% glycerol and 0.3% casamino acids) in duplicate 96-well, flat bottom, polyvinyl chloride microtiter plates (Falcon; BD Biosciences, San Jose, CA). Following 24 h static incubation at 37 °C, wells were washed, and the biofilm attached to well surfaces was stained with 0.1% (wt/vol) crystal violet solution (Sigma-Aldrich). Following washing, the bound crystal violet was solubilized from adherent cells with 33% acetic acid and subsequently quantified by measuring the optical density at 595 nm. The data for each strain represent average values taken from four replicate wells performed in two independent experiments.

Bacterial Sample Preparation for AFM Measurements. Samples for AFM measurements were prepared as previously described.[18] Briefly, either polyethylenimine (PEI)-coated or gelatin-coated glass disks were used to immobilize bacteria, since capsule-deficient bacteria could not firmly adhere to PEI-coated glass disks to meet the requirements for force measurement. PEI-coated glass disks were prepared by exposing 0.5 mL of a PEI solution (0.005% w/v) to a freshly prepared glass disk for 4 h. Gelatin-coated glass disks were prepared by submerging glass disks in a gelatin/chromium solution for 1 min, and then slowly removing and standing upright at room temperature overnight under sterile conditions. After coating with either PEI or gelatin, disks were rigorously rinsed with Milli-Q water and air-dried under sterile conditions, prior to cell deposition. Bacteria were immobilized by depositing a drop of cell suspension onto the disk. The sample was left for 1.5 h at room temperature to allow cells to adhere, then rinsed gently with Milli-Q water to remove any nonadherent cells, and then immediately immersed in Milli-Q water and mounted immediately into the AFM for measurement.

Atomic Force Microscopy. All AFM measurements on live bacteria were carried out in Milli-Q water at room temperature using an MFP-3D instrument (Asylum Research, Santa Barbara, CA). Silicon nitride cantilevers were purchased from Veeco (MLCT, Santa Barbara, CA) with a nominal spring constant of 0.01 N/m and a nominal probe curvature radius of 20 nm (provided by the manufacturer). Cantilever spring constants were calibrated using a thermal tune function contained in the MFP 3D software (Asylum Research, Santa Barbara, CA). All tips were cleaned in a BioForce UV/ozone cleaner (BioForce Nanosciences, Inc., Ames, IA) for 15 min before use. The photodetector sensitivity was calibrated on a PEI-coated surface using standard protocols.[13] The slope of the constant compliance region of the force curves obtained on the PEI-coated glass disk was used to convert the deflection (D) in millivolts to nanometers.[13] The cantilever deflection was then converted into a force (F) according to $F = k \times D$, where k is the force constant of the cantilever.[21] Nanomechanical measurements were performed by collecting a set of force curves on the apex of individual cells to avoid side-on interactions, at a loading rate of 2 μm s^{-1}. To ensure the force profiles were repeatable and representative of the population of cells, measurements were taken on at least 10 different points along the apex of an individual cell, for at least 7 cells in a sample. For each cell type, this was performed on 5–7 separate sample preparations. Force curves measured in this way on individual bacteria are highly reproducible (Supporting Information Figure S1). Igor Pro (Version 6.04, Wavemetrics Inc.) routines were written for data analysis.[18] Radmacher et al. reported that there is negligible variation in the AFM tips if using the same types of cantilever from the same batch.[21] In our experiments, the same types of cantilever from the same batch were used. Cells were imaged prior to and after force measurements to ensure no change to cell morphology.

Force Profile Fitting. To analyze the force profiles, it is essential to determine the point of contact, i.e., zero tip–sample distance. Under the experimental conditions used here, there is a long-range double layer interaction between the tip and the bacterial cell surface. The contact is defined as the piezo displacement where a force–distance curve deviates from double layer theory.[17,22] If there is no observable long-range force, the contact is defined as the point on the force profile where the cantilever starts to deflect upward.[13] Raw force curves were converted into force versus tip-to-sample distance curves for which negative values correspond to cell indentation and positive values correspond to long-range noncontact interactions. From the compressive part of the force profile, nanomechanical properties of a bacterial cell can be extracted to yield information on the structure and organization of the capsule polysaccharides, cell wall, and turgor pressure, as previously described[18] and outlined below.

RESULTS AND DISCUSSION

Contact mode AFM was used to image live bacterial cells before and after force measurements. Figure 1 shows a typical image of individual *K. pneumoniae* cells in Milli-Q water. The cell topography is homogeneous and remains such after force measurement.

As previously described,[18] information on the organizational structure of the bacterial cell envelope can be obtained by fitting different regimes of the force profiles to an appropriate

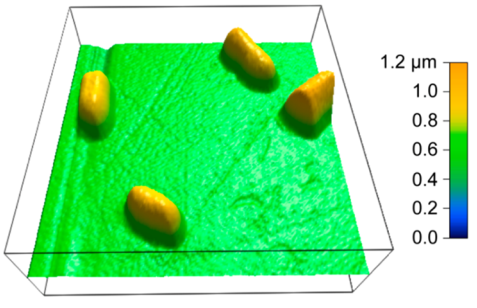

Figure 1. Bacterial morphology. AFM contact-mode 3D height image of wild type *K. pneumoniae* AJ218 cells attached to the surface of a PEI-coated glass disk in Milli-Q water. Scan size: 8 μm × 8 μm.

DOI: 10.1021/acsami.5b03041
ACS Appl. Mater. Interfaces 2015, 7, 13007–13013

theory of cell−tip interaction using a mechanical model that describes localized cell indentation. The model is based on the characteristic form of the measured force profiles and what is understood about the bacterial cell envelope with capsule. Typical force profiles on wild type *K. pneumoniae* are shown in Figure 2. As previously reported,[18] the data contain four major

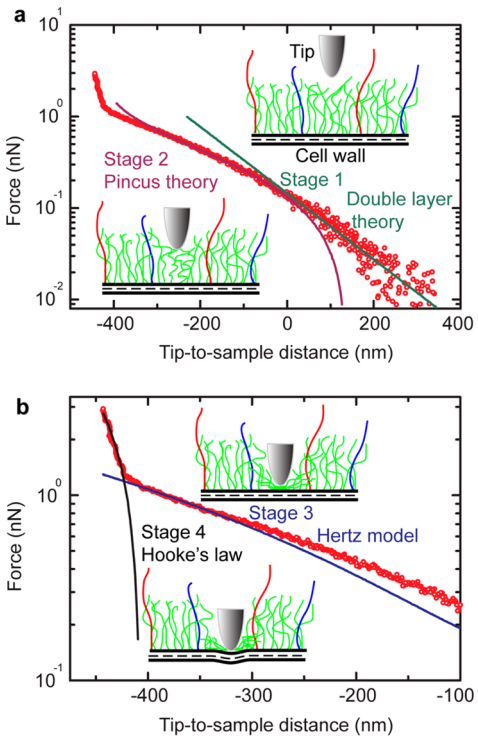

Figure 2. Four-stage model of force profile analysis on a semilog scale. (a) A typical force profile for the interaction between an AFM tip and individual wild type *K. pneumoniae* AJ218 bacterial cells. The compressive region of this force profile from −100 to −450 nm is shown in part b for clarity. The solid lines are the lines of best fit to the data (red) for different regions of the force profile. Stage 1 (long-range noncontact interaction) is best fitted by double layer theory (green line). Stage 2, capsule compression, is best fitted by the Pincus model of polyelectrolyte brush compression (purple line). Stage 3, deformation of compacted surface polymers, is well fitted by the Hertz model (blue line), and stage 4, compression of the cytoplasm, is well-fitted by Hooke's law (black line). The cell wall comprises the outer membrane, the thin peptidoglycan layer (dashed), and the cytoplasmic membrane. Capsular polysaccharides (green lines), type 3 fimbriae (red lines), and other fimbriae types (blue lines) cover the cell wall.

stages of cell indentation for encapsulated *K. pneumoniae* cells. For clarification, the corresponding theories and equations of the four stages used in data fitting are given in Table 1.

Stage 1 is a long-range double layer interaction between the bacterial surface and the AFM probe. The average value of the Debye length for wild type *K. pneumoniae* in Milli-Q water is 111 nm, in good agreement with that expected in pure water (~100 nm).

The double layer interaction dominates the net force until the approaching probe makes contact with the cell surface marking the onset of stage 2: compression of the bacterium's surface polymers where the force is dominated by steric and/or electrosteric interactions.[17,22,23] The force profile over this range (from 0 to −296 nm in the example force profile) is well-fitted by the Pincus theory for compression of a polyelectrolyte brush.[17,22,23] Fitting the force profile to indentation, δ, in response to an applied loading force, $F_{loading}$, using the Pincus theory (see eq 1 in Table 1),[22] gives an estimate of total capsule thickness i.e., $-\delta_L^0$, and δ_L^0 is the onset of linear compliance. In Pincus theory, A_p is given by eq 2 in Table 1.[17,22]

In our experiments, the temperature is constant so the magnitude of A_p is determined by the ratio N_B/d^2. Since pH and electrolyte concentration are constant from experiment to experiment, we assume N_B is approximately constant, and so any change to N_B/d^2 is due to a change in the capsule density. The range of the force profile over which the Pincus theory fits the data from tip-to-sample contact is the distance over which the capsule is brush-like, which approximates 296 nm as shown in Figure 2.

Stage 3 occurs when the compacted brush-like structure of the bacterial capsule is further altered under a positive loading force. This interaction (from −296 to −407 nm in the example force profile) is well-fitted by Hertz's model (see eq 3 in Table 1)[24−26] to obtain the elastic modulus, E, of the compressed polymer layer and cell wall. In the present experiments, υ was set to 0.5, as commonly used in AFM measurements,[21] and α was set to 35°, according to the AFM tip manufacturer's specifications (Application Note #141, Bruker). This suggests that, over this regime of nanoindentation, the bacterial surface responds like an elastic body to an increased applied load.

Stage 4 occurs when the loading force is predominantly opposed by the cell cytoplasmic turgor, as the cell is indented by an amount, δ. This region of the force profile can be well fitted by Hooke's law (see eq 4 in Table 1)[17,21] where $K_{bacterium}$ is a measure of the cell cytoplasmic turgor pressure.

A comparison was made between the mechanical properties of wild type and capsule-deficient *K. pneumoniae* (Figure 3). These profiles clearly highlight the effect of the capsule in protecting the cell from mechanical perturbation. The nonlinear repulsive force extending over 400 nm in the compressive region seen in the wild type is absent in the capsule-deficient strain. This indicates that type 3 fimbriae (including other fimbrial types) of this *K. pneumoniae* strain that are expressed in the absence of the capsule offer a negligible barrier to cell compression, and the resistance to compression observed in the wild type strain is due to the presence of the capsule. The long-range repulsive double layer interaction between the negatively charged AFM tip and the wild type bacterial cells is absent with the capsule-deficient bacteria. This suggests that the net negative charge on the bacteria originates from the polysaccharide capsule and that there is a negligible contribution to the net charge from the fimbriae and lipid in the outer membrane, consistent with previous studies.[27,28] For the capsule-deficient bacteria, a jump into contact from approximately 50 nm tip-to-sample distance was observed (Figure 3, inset). This long-range attraction between the tip and the bacterial cell surface is unlikely to be a bridging interaction due to the fimbriae, since the length of the fimbriae (~hundreds of nanometers) is an order of magnitude larger than the range of the attraction. It is therefore likely to be a van der Waals attraction or polymer bridging between lipopolysaccharide and the AFM tip.

Typical force profiles for the interaction between an AFM tip and individual wild type *K. pneumoniae* cells and various mutants are shown in Figure 4. The *K. pneumoniae* AJ218-derived isolates selected for comparison were (i) a type 3 fimbriae-deficient mutant, (ii) a type 3 fimbriae overexpressed

DOI: 10.1021/acsami.5b03041
ACS Appl. Mater. Interfaces 2015, 7, 13007−13013

Table 1. Summary of the Four-Stage Nanomechanics Model Used for the Analysis of Force Profiles Obtained in the Compression Process[a]

stage	model	equation	fitting parameters
stage 1	double layer force	exponential fitting	Debye length
stage 2	Pincus theory	$F_{\text{loading}} = A_{\text{p}} \ln\left(\frac{\delta_{\text{L}}^{0}}{\delta_{\text{L}}^{0} - \delta}\right)$ (1)	A_{p}
		$A_{\text{p}} \propto \frac{4\pi k_{\text{B}} T N_{\text{B}}}{d^2}$ (2)	
stage 3	Hertz model	$\frac{\partial F_{\text{loading}}}{\partial \delta} = \left[F_{\text{loading}} \frac{E}{(1-\upsilon^2)} 2\pi \tan(\alpha)\right]^{1/2}$ (3)	E
stage 4	Hooke's law	$F_{\text{loading}} = K_{\text{bacterium}} \delta$ (4)	$K_{\text{bacterium}}$

[a] F_{loading}, loading force; δ, indentation; δ_{L}^{0}, the onset of linear compliance; A_{p}, prefactor; d, the grafted interchain distance of the brush; N_{B}, the number of monomers carrying ionic charge; k_{B}, Boltzmann's constant; T, temperature; E, elastic modulus; υ, the Poisson ratio; α, half-opening angle of the cone indenter; $K_{\text{bacterium}}$, the spring constant of the bacterium.

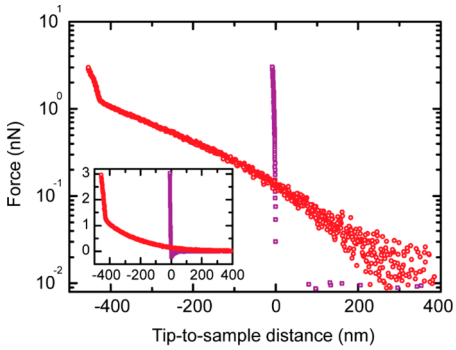

Figure 3. Typical force profiles plotted on a semilog scale for the interaction between an AFM tip with wild type (red) and capsule-deficient (purple) live *K. pneumoniae* AJ218 bacterial cells in Milli-Q water. The inset shows the respective force profiles on a linear scale.

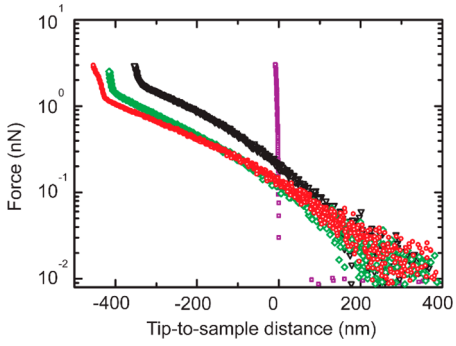

Figure 4. Typical force of interaction between an AFM tip and individual, live wild type (red), type 3 fimbriae overexpressed (green), type 3 fimbriae-deficient (black), and capsule-deficient (purple) *K. pneumoniae* AJ218 bacteria, *in situ*.

strain, and (iii) a capsule-deficient mutant. These isolates facilitated an investigation of the role of type 3 fimbriae, a required surface structure that mediates *K. pneumoniae* biofilm formation,[8] on the nanomechanics and biofilm formation of *K. pneumoniae*. The capsule-deficient bacteria has a force profile that is distinct from the others, due to the absence of a thick, compressible capsule, discussed above. The forms of the indentation regimes (negative tip-to-sample distance values) of the wild type, fimbriae overexpressed and fimbriae-deficient bacteria are somewhat similar and are well-fitted using our four-stage model of bacterial cell indentation, described above and as shown in Figure 2 (for wild type) and Figures S2 (for fimbriae overexpressed) and S3 (for fimbriae-deficient) in Supporting Information. Each exhibits a double layer interaction between the bacterial cells and the AFM tip with average Debye lengths of 111, 107, and 121 nm, respectively, in reasonable agreement with that expected in pure water (~100 nm). The data extracted from the fits to the compressive regions of the force profiles are given in Table 2. The local spring constant of a bacterial cell, $K_{\text{bacterium}}$ (i.e., turgor pressure), was determined from the slope of the linear portions of the force profiles using eq 4 in Table 1. These values are comparable to previous studies for Gram-negative bacteria such as *Escherichia coli* strains (~40 mN/m)[13] and *Shewanella* bacterial strains from ~60 to ~130 mN/m, depending on aqueous solution conditions.[17] We have previously shown that, under the same conditions, no change in cell viability is observed over the course of an experiment.[18]

Table 2. Summary of Physical Parameters Extracted from the Fits to the Force Profiles Using the Nanomechanical Model for Bacterial Cell Indentation for Wild Type, Type 3 Fimbriae-Deficient, and Type 3 Fimbriae Overexpressed *K. pneumoniae* AJ218 Bacteria[a]

model and stage	physical parameter	wild type	fimbriae-deficient	fimbriae overexpressed
double layer theory (stage 1)	Debye length (nm, ±10%)	111	107	121
Pincus theory (stage 2)	total capsule thickness (nm, ±10%)	420	395	401
	brush thickness (nm, ±10%)	282	202	286
	relative capsule density (±0.1)	1.7	1.2	1.7
Hertz model (stage 3)	compacted surface polymers' elastic modulus (kPa, ±0.2)	5.5	7.4	6.3
Hooke's law (stage 4)	relative cell turgor pressure (mN/m, ±10%)	74	116	100

[a] Numbers quoted are averages from 350−490 force profiles.

The data in Table 2 show that loss of fimbriae affects capsule structure. The capsule indentation regime of the force profile for the wild type, type 3 fimbriae-deficient and type 3 fimbriae overexpressed bacteria are all well-fitted to the Pincus theory

DOI: 10.1021/acsami.5b03041
ACS Appl. Mater. Interfaces 2015, 7, 13007−13013

for polymer brush compression. The total capsule thicknesses for the wild type, type 3 fimbriae-deficient and type 3 fimbriae overexpressed bacteria lie within experimental error of each other. It might be expected that the absence of type 3 fimbriae would lead to a degree of capsule collapse since the total number of polymers on the cell surface decreases. However, the capsule of the fimbriae-deficient bacteria was not observed to collapse at all, considering the unaltered capsule thickness. Interestingly though, the capsule of the fimbriae-deficient bacteria is significantly less brush-like in organization than the wild type and fimbriae overexpressed strains (brush length 202 nm versus 282 and 286 nm) which have very similar structures. It is tempting to explain this as being due to a collapse of brush structure brought about by a reduction in fimbriae. However, as already discussed, there is no reduction in the total capsule thickness. This is consistent with the reduction in capsule density that results from fimbriae deficiency.

Another important observation from the data in Table 2 is the comparison of the elastic or Young's modulus for the three bacterial strains. The type 3 fimbriae-deficient bacteria have a significantly more rigid cell surface structure compared to the wild type, and fimbriae overexpressed bacteria. This seems to contradict the data obtained for the structure of the capsule. The less dense capsule of the fimbriae-deficient bacteria should be easier to compress. The data however suggest that the altered capsular structure of the fimbriae-deficient strain instead leads to a more rigid cell surface structure, even though the total density of the capsule is less than that of the wild type and fimbriae overexpressed strains. A possible explanation for these results is that, with removal of the type 3 fimbriae, the capsular polysaccharides can form a more organized and interconnected network through inter- and intra-segment hydrogen bonding.[29] This is illustrated schematically in Figure 5. Such a structure will entrain more water to maintain polysaccharide hydration, as is typical of a cross-linked polymer hydrogel, but will be more difficult to compress than a polymer brush due to the energetic cost of disrupting the interconnected network. This explanation is consistent with the work of Ou et al.,[30] who found that shearing polymer hydrogel layers does not lead to a breaking of the network and chain interpenetration and so results in a low coefficient of friction compared to that for polymer brush layers, which are able to interpenetrate.

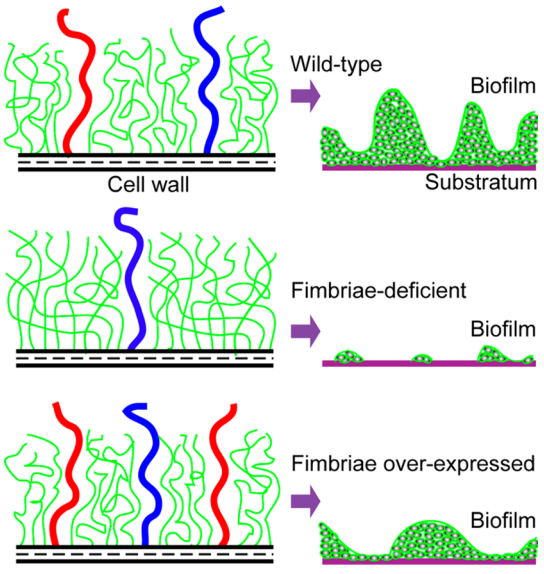

Figure 5. Organization of the capsule of the wild type (top panel), type 3 fimbriae-deficient (middle panel), and type 3 fimbriae overexpressed (bottom panel) *K. pneumoniae* AJ218 bacteria influences cell surface adhesion, and thereby biofilm formation. The green lines, red lines, and blue lines represent capsular polysaccharides, type 3 fimbriae, and other fimbriae types, respectively.

These results have important implications in bacterial cell adhesion, since the more ordered and so less fluid the capsular polysaccharides, the less able they are to form strong points of adhesion to a substrate, since energy is required to break the organized structure in the process of bacterial cell attachment to a surface.[31] The existence of a better organized structure on the type 3 fimbriae-deficient bacteria should impede biofilm formation. To test this hypothesis, we compared the ability to form static biofilms of all bacterial strains studied here plus a wild type with empty vector as a control. The results of these standard microtiter plate biofilm assays are shown in Figure 6.

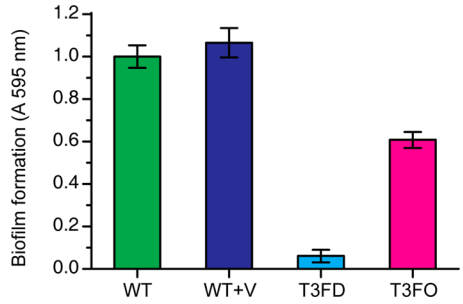

Figure 6. Microtiter plate assay results for the formation of biofilm by *K. pneumoniae* AJ218 wild type (WT), wild type plus empty expression vector (WT + V), type 3 fimbriae-deficient (T3FD) mutant, and type 3 fimbriae overexpressed (T3FO) strains. The microtiter plate assay was performed for 24 h under static conditions. The error bars represent the standard deviation. Statistical significance between AJ218 wild type and isogenic mutants was analyzed by one-way ANOVA and Tukey HSD post hoc comparisons. All *P* values (T3FD and T3FO compared to WT) are smaller than 0.001.

The removal of the type 3 fimbriae resulted in a significant impairment in biofilm formation on an abiotic surface compared with that of the wild type, while overexpression of type 3 fimbriae led to relatively modest impairment in biofilm formation. The control (empty) bacterial expression vector used to drive overexpression of fimbriae through over-expression of the type 3 fimbriae genes did not have any significant impact on biofilm formation (WT + V, Figure 6).

The reduction in biofilm-forming ability seen in the fimbriae-deficient mutants (Figure 6) cannot be simply attributed to the removal of the type 3 fimbriae themselves, since, by this same reasoning, an overexpression of these fimbriae should lead to an enhancement in biofilm formation compared with that of the wild type. What we found, however, is that the fimbriae overexpressed strain produced less biofilm than the wild type bacteria. It therefore follows that the more highly organized, less fluid capsular structure of the fimbriae-deficient mutants may inhibit biofilm formation. The overexpression of fimbriae still allows for fluidity of the capsular polysaccharides and adhesion to a surface via the capsule, but with some steric hindrance presented by the additional fimbriae, compared with the wild type bacteria. It is known that steric hindrance can inhibit the function of short bacterial adhesins in *E. coli*.[32] It should be pointed out that the capsule organization may not play a major role in processes that involve specific interactions

DOI: 10.1021/acsami.5b03041
ACS Appl. Mater. Interfaces 2015, 7, 13007−13013

such as adhesin−receptor interactions, as occur in host−cell interactions.

CONCLUSIONS

In summary, we found that the type 3 fimbriae help maintain the fluidity of the polysaccharide capsule in the bacterial species *Klebsiella pneumoniae*. This fluidity is essential for optimal cell adhesion to a surface and efficient biofilm formation in this species. The type 3 fimbriae ensure this fluidity by minimizing hydrogen bonding interconnection between the capsular polysaccharide molecules. In the absence of type 3 fimbriae, the capsule forms a more rigid interconnected hydrogel structure, and biofilm formation is severely limited. The overexpression of type 3 fimbriae can slightly limit biofilm formation by steric overcrowding on the cell surface. We therefore conclude from this study that the organization of the capsule plays an important role in biofilm formation. These insights can potentially assist in the development of strategies to prevent biofilm formation on medical devices.

ASSOCIATED CONTENT

Supporting Information

Force curve reproducibility (Figure S1); theoretical fitting of the mechanical data for the type 3 fimbriae overexpressed (Figure S2) and the type 3 fimbriae-deficient (Figure S3) mutants of *K. pneumoniae* cells. The Supporting Information is available free of charge on the ACS Publications website at DOI: 10.1021/acsami.5b03041.

AUTHOR INFORMATION

Corresponding Author

*E-mail: rastru@unimelb.edu.au.

Notes

The authors declare no competing financial interest.

ACKNOWLEDGMENTS

The authors gratefully acknowledge the support of the Melbourne Materials Institute for interdisciplinary seed funding for this project. In addition, this work was supported by the Australian Government National Health and Medical Research Council (NHMRC) Project Grant 628770, NHMRC Program Grant 606788, and Australian Research Council Project Grant DP130100957. H.W. also acknowledges the support from NSFC (No. 11105090), CIGIT for Startup Foundation for Advanced Talents, Chongqing Science and Technology Commission (cstc2013yykfC00007 and cstc2013jcyjC00001), and the Chinese Academy of Sciences for a Key Scientific Instrument and Equipment Development Project.

REFERENCES

(1) Schroll, C.; Barken, K. B.; Krogfelt, K. A.; Struve, C. Role of Type 1 and Type 3 Fimbriae in *Klebsiella pneumoniae* Biofilm Formation. *BMC Microbiol.* **2010**, *10*, 179.

(2) Roberts, I. S. The Biochemistry and Genetics of Capsular Polysaccharide Production in Bacteria. *Annu. Rev. Microbiol.* **1996**, *50*, 285−315.

(3) Donlan, R. M. Biofilm Formation: A Clinically Relevant Microbiological Process. *Clin. Infect. Dis.* **2001**, *33*, 1387−1392.

(4) Podschun, R.; Ullmann, U. *Klebsiella Spp*. as Nosocomial Pathogens: Epidemiology, Taxonomy, Typing Methods, and Pathogenicity Factors. *Clin. Microbiol. Rev.* **1998**, *11*, 589−603.

(5) Schembri, M. A.; Blom, J.; Krogfelt, K. A.; Klemm, P. Capsule and Fimbria Interaction in *Klebsiella pneumoniae*. *Infect. Immun.* **2005**, *73*, 4626−4633.

(6) Jagnow, J.; Clegg, S. *Klebsiella pneumoniae* MrkD-Mediated Biofilm Formation on Extracellular Matrix- and Collagencoated Surfaces. *Microbiology* **2003**, *149*, 2397−2405.

(7) Ubbink, J.; Schar-Zammaretti, P. Probing Bacterial Interactions: Integrated Approaches Combining Atomic Force Microscopy, Electron Microscopy and Biophysical Techniques. *Micron* **2005**, *36*, 293−320.

(8) Wilksch, J. J.; Yang, J.; Clements, A.; Gabbe, J. L.; Short, K. R.; Cao, H. W.; Cavaliere, R.; James, C. E.; Whitchurch, C. B.; Schembri, M. A.; Chuah, M. L. C.; Liang, Z. X.; Wijburg, O. L.; Jenney, A. W.; Lithgow, T.; Strugnell, R. A. MrkH, A Novel C-Di-GMP-Dependent Transcriptional Activator, Controls *Klebsiella pneumoniae* Biofilm Formation by Regulating Type 3 Fimbriae Expression. *PLoS Pathog.* **2011**, *7*, e1002204.

(9) Otto, K. Biophysical Approaches to Study the Dynamic Process of Bacterial Adhesion. *Res. Microbiol.* **2008**, *159*, 415−422.

(10) Dufrene, Y. F. Atomic Force Microscopy and Chemical Force Microscopy of Microbial Cells. *Nat. Protoc.* **2008**, *3*, 1132−1138.

(11) Muller, D. J.; Dufrene, Y. F. Atomic Force Microscopy as A Multifunctional Molecular Toolbox in Nanobiotechnology. *Nat. Nanotechnol.* **2008**, *3*, 261−269.

(12) Gaboriaud, F.; Dufrene, Y. F. Atomic Force Microscopy of Microbial Cells: Application to Nanomechanical Properties, Surface Forces and Molecular Recognition Forces. *Colloids Surf., B* **2007**, *54*, 10−19.

(13) Velegol, S. B.; Logan, B. E. Contributions of Bacterial Surface Polymers, Electrostatics, and Cell Elasticity to the Shape of AFM Force Curves. *Langmuir* **2002**, *18*, 5256−5262.

(14) Wright, C. J.; Armstrong, I. The Application of Atomic Force Microscopy Force Measurements to the Characterisation of Microbial Surfaces. *Surf. Interface Anal.* **2006**, *38*, 1419−1428.

(15) Francius, G.; Lebeer, S.; Alsteens, D.; Wildling, L.; Gruber, H. J.; Hols, P.; De Keersmaecker, S.; Vanderleyden, J.; Dufrene, Y. F. Detection, Localization, and Conformational Analysis of Single Polysaccharide Molecules on Live Bacteria. *ACS Nano* **2008**, *2*, 1921−1929.

(16) Hinterdorfer, P.; Dufrene, Y. F. Detection and Localization of Single Molecular Recognition Events Using Atomic Force Microscopy. *Nat. Methods* **2006**, *3*, 347−355.

(17) Gaboriaud, F.; Gee, M. L.; Strugnell, R.; Duval, J. F. L. Coupled Electrostatic, Hydrodynamic, and Mechanical Properties of Bacterial Interfaces in Aqueous Media. *Langmuir* **2008**, *24*, 10988−10995.

(18) Wang, H. B.; Wilksch, J. J.; Lithgow, T.; Strugnell, R. A.; Gee, M. L. Nanomechanics Measurements of Live Bacteria Reveal A Mechanism for Bacterial Cell Protection: the Polysaccharide Capsule in *Klebsiella* Is A Responsive Polymer Hydrogel That Adapts to Osmotic Stress. *Soft Matter* **2013**, *9*, 7560−7567.

(19) Jenney, A. W.; Clements, A.; Farn, J. L.; Wijburg, O. L.; McGlinchey, A.; Spelman, D. W.; Pitt, T. L.; Kaufmann, M. E.; Liolios, L.; Moloney, M. B.; Wesselingh, S. L.; Strugnell, R. A. Seroepidemiology of *Klebsiella pneumoniae* in An Australian Tertiary Hospital and Its Implications for Vaccine Development. *J. Clin. Microbiol.* **2006**, *44*, 102−107.

(20) de Lorenzo, V.; Herrero, M.; Jakubzik, U.; Timmis, K. N. Mini-Tn5 Transposon Derivatives for Insertion Mutagenesis, Promoter Probing, and Chromosomal Insertion of Cloned DNA in Gram-Negative Eubacteria. *J. Bacteriol.* **1990**, *172*, 6568−6572.

(21) Radmacher, M.; Fritz, M.; Hansma, P. K. Imaing Soft Samples with the Atomic Force Microscope: Gelatin in Water and Propanol. *Biophys. J.* **1995**, *69*, 264−270.

(22) Considine, R. F.; Drummond, C. J.; Dixon, D. R. Force of Interaction between A Biocolloid and An Inorganic Oxide: Complexity of Surface Deformation, Roughness, and Brushlike Behavior. *Langmuir* **2001**, *17*, 6325−6335.

(23) Abraham, T.; Giasson, S.; Gohy, J. F.; Jerome, R. Direct Measurements of Interactions between Hydrophobically Anchored

DOI: 10.1021/acsami.5b03041
ACS Appl. Mater. Interfaces 2015, 7, 13007−13013

Strongly Charged Polyelectrolyte Brushes. *Langmuir* **2000**, *16*, 4286−4292.
(24) Radmacher, M. Measuring the Elastic Properties of Biological Samples with the AFM. *IEEE Eng. Med. Biol. Mag.* **1997**, *16*, 47−57.
(25) Hertz, H. R. On Contact between Elastic Bodies. *Mathematik* **1882**, *92*, 156−171.
(26) Oyen, M. L. Nanoindentation of Biological and Biomimetic Materials. *Exp. Tech.* **2013**, *37*, 73−87.
(27) Muratsugu, M.; Miyake, Y.; Ishida, N.; Hyodo, A.; Terayama, K. Decrease in Surface Charge Density of *Klebsiella-pneumoniae* Treated with Cefodizime and Enhancement of the Phagocytic Function of Human Polymorphonuclear Leukocytes Stimulated by the Drug-treated Bacteria. *Biol. Pharm. Bull.* **1995**, *18*, 1259−1263.
(28) Camprubi, S.; Merino, S.; Benedi, J.; Williams, P.; Tomas, J. M. Physicochemical Surface-Properties of *Klebsiella-pneumoniae*. *Curr. Microbiol.* **1992**, *24*, 31−33.
(29) Mayer, C.; Moritz, R.; Kirschner, C.; Borchard, W.; Maibaum, R.; Wingender, J.; Flemming, H. C. The Role of Intermolecular Interactions: Studies on Model Systems for Bacterial Biofilms. *Int. J. Biol. Macromol.* **1999**, *26*, 3−16.
(30) Ou, Y. P.; Sokoloff, J. B.; Stevens, M. J. Discrete Model Studies of Two Grafted Polyelectrolyte Polymer Hydrogels Pressed in Contact. *J. Chem. Phys.* **2013**, *139*, 144902.
(31) Zhang, C.; Hankett, J.; Chen, Z. Molecular Level Understanding of Adhesion Mechanisms at the Epoxy/polymer Interfaces. *ACS Appl. Mater. Interfaces* **2012**, *4*, 3730−3737.
(32) Schembri, M. A.; Dalsgaard, D.; Klemm, P. Capsule Shields the Function of Short Bacterial Adhesins. *J. Bacteriol.* **2004**, *186*, 1249−1257.

DOI: 10.1021/acsami.5b03041
ACS Appl. Mater. Interfaces 2015, 7, 13007−13013